COMPOSITE MATERIAL DAMAGE MONITORING USING EMBEDDED IN POLYMER MATRIX OPTICAL FIBER BRAGG GRATING OR LONG PERIOD GRATING SENSORS

Dan SAVASTRU [1], Sorin MICLOS[2], Roxana SAVASTRU[3], Florina-Gianina ELFARRA[4], and Ion LANCRANJAN[5]

A new method of detecting how a crack appears and grows, as a damage, in fiber reinforced polymer composite material using embedded Fiber Bragg Grating (FBG) and/or Long Period Grating Fiber Sensors (LPGFS) is presented. Different features of the crack mechanism that induce a change in the FBG sensor or LPGFS response are identified. The response of FBG sensor or LPGFS under host composite material host crack action is investigated and simulated for defining the functional limits of the composite material. FBG sensor or LPGFS are considered as embedded in polymer matrix of composite material.

Keywords: Fiber Bragg Grating, Long Period Grating, Composite Damage.

1. Introduction

The use of composite components in the aerospace and in the automotive fields field is increasing gradually due to the opportunities they present for high specific stiffness and strength, weight reduction, fatigue performance, improved thermal and electrical conductivity and the possibility to integrate sensors or actuators [1-10]. Due to the composition complexity of composite material, its final properties depend on the properties of component materials (polymer matrices, reinforcements, fillers and additives). A combination of parameters affects the design with composite materials, including the number of layers, the material combinations, ply directions and fabrication method. A variety of methods are available nowadays for composite materials manufacturing, such as vacuum, autoclave, Resin Transfer Molding (RTM) and Liquid Resin Infusion (LRI) [1-10].

Most efficient use of advanced composites in aerospace and automotive lead to the introduction of Structural Health Monitoring (SHM) concept which aims to give, at every moment during the life of a structure, a diagnosis of the

[1]Dr. Eng., National Institute of R&D for Optoelectronics- INOE 2000, Romania, e-mail: dsavas@inoe.ro
[2] Eng., National Institute of R&D for Optoelectronics- INOE 2000, Romania, e-mail: miclos@inoe.ro
[3] Dr. Eng., National Institute of R&D for Optoelectronics- INOE 2000, Romania, e-mail: rsavas@inoe.ro
[4] Phys., "Saint John" Emergency Clinical Hospital e-mail: gianina.elfarra@gmail.com
[5] Phys., National Institute of R&D for Optoelectronics- INOE 2000, Romania, e-mail: ion.lancranjan@inoe.ro

status of the constituent materials, of the different parts, and of the full assembly of these parts constituting the structure as a whole" [1-10]. Or, alternatively, SHM is defined as the use of in-situ, non-destructive sensing and analysis of structural characteristics, including the structural response, for detecting changes that may indicate damage or degradation [8-10]. Starting from a recent alternative definition of SHM given by NASA and consisting of using the concept of Fault Management, which is defined as "the operational capability of a system to contain, prevent, detect, diagnose, respond to, and recover from conditions that may interfere with nominal mission operations [10].

Many definitions have been proposed to describe damage, health and structural monitoring. In general, health is defined as the ability to function and maintain the structural integrity during the entire life of a structure. Damage can be defined as a material, structural or functional failure, or as a change in physical parameters, such as mass, stiffness or damping. Monitoring is the process of structural diagnosis and prognosis [1-10]. SHM is considered as the observation of a system over time based on periodically sampled response measurements from a sensor network, the extraction of features sensitive to damage and the analysis of these features, in order the system's structural condition - health to be defined [1-10]. It consists a very important tool for the current and future design, analysis and maintenance of engineering structures [8]. SHM is important in applications with highly loaded parts, areas susceptible to corrosion and in applications with high fatigue loads [10]. The SHM is strongly related with the concept of defects induced in the investigated. Basically, SHM is a measure of detecting defects which are induced into the composite materials [1-15]. Voids, delamination of polymer matrix composite material are the principal cause of SHM use. Concerning the use of embedded into polymer matrix of composite material of FBG and/or LPGFS for detection, for accomplishing SHM, of defects induced into the composite material structure it is accepted that bending of optical fiber sensors is the main process affecting FBG and/or LPGFS characteristics. Optical fiber bending means changes into the polarization status of the light guided through the optical fiber, which signifies that birefringence is induced into optical fiber.

2. Theory

In Figs. 1 and 2 there are presented schematically the processes related to the bending of optical fiber [11-19]. Fibers in practical devices and systems are always bent in some way and some degree. It was found early in the 1970s that fiber bending would cause birefringence, which was explained theoretically in the literature. An analysis of the stress and strain states in bent single mode fibers allows the deduction of the related formulas by photo-elastic effect and explain experimental phenomena [14, 15]. A bent fiber can be considered a bent

cylindrical silica rod. Fig. 1 shows a section of fiber, which is not only bent but also stretched, because bending and axial deformations occur often simultaneously. In a tension-coiled fiber a pressure from a cylindrical support must be applied on the fiber at its inner side of bending to balance the axial stretching force. A neutral surface exists inside the rod, at $x = -x_0$ in Fig. 1, on which there is no axial extension, nor does the compression occur; that is the fiber length on the neutral surface is equal to its original length under no bending and no stretching. In case of pure bending, without any axial stretching, the neutral surface passes through the fiber axis, at $x_0 = 0$. It is shown that the part above the neutral surface suffers stretching axially, whereas the part beneath is compressed. The axial strain is expressed approximately as a linear function of x, measured from the neutral surface, with a coefficient proportional to the bending curvature 1/R. Under the first-order approximation, the averaged axial strain caused by an axial stress is calculated as a function of optical fiber diameter and bending curvature. The defined formula gives the dependence of neutral surface position on the axial stress. The basic effect found in bent fiber experimentally is birefringence. Obviously, mere axial strain cannot explain the phenomenon. It is necessary to analyze the transverse deformation of the bent fiber. It is conjectured that the round rod is deformed to be an elliptical rod and asymmetric strain occurs around the center of curvature. To reveal the mechanism, we must understand the transverse distribution of stress and strain inside the fiber. To solve the elastic state of bent fiber some approximations are made. Birefringence induced by bending the optical fiber is observed as spectral shifting and splitting of the reflection band in the case of FBG and of the absorption bands in the case of LPGFS. The main idea to be highlighted consists of the simple observation that any so-called hidden damage appeared in the structure of a polymer composite material will produce a bending of the FBG sensor or LPGFS [11-19].

Second, any component of strain and stress is not a function of axial position z, when a uniform curvature bending is considered. Then the three-dimensional problem is reduced to a two-dimensional deformation problem. The shearing forces σ_{xz} and σ_{yz}, induced by bending, are regarded as equivalent body forces in the transverse cross-sectional plane, which has only one component in x direction, expressed as a mathematical function [11-19].

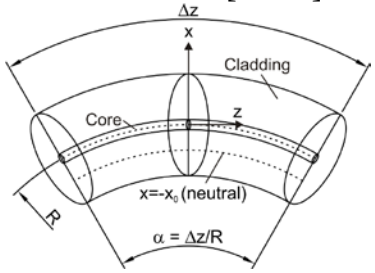

Fig. 1. Bent and stretched optical fiber.

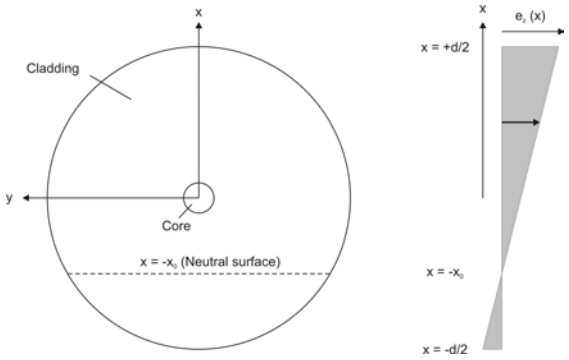

Fig. 2. Strain distribution in the bent optical fiber.

For pure bending, the axial strain is expressed approximately as a linear function of *x*, measured from the neutral surface, with a coefficient proportional to the bending curvature 1/*R* [11-19]:

$$e_z = \frac{x + x_0}{R} \tag{1}$$

Considering the first-order approximation for an optical fiber with the diameter *d* and the Young modulus Y, the averaged axial strain caused by an axial stress is defined as

$$\overline{\sigma}_z = \frac{4Y}{\pi d^2} \int e_z dxdy = \frac{Y}{R} x_0 = Y\overline{e}_z \tag{2}$$

Eq. (2) is important as it gives the dependence of neutral surface position on the axial stress. The above described axial strain and the stress distribution are the first-order one and defined as:

$$\sigma_z^{(1)} = Ye_z = \frac{Y}{R}\left(x + x_0\right) \tag{3}$$

Then, considering the three-dimensional problem as a two-dimensional plane deformation problem, in the second-order approximation, the shearing force σ_{xz} and σ_{yz}, induced by bending, is regarded as an equivalent body force in the transverse cross-sectional plane, which has only one component in *x* direction, expressed as

$$F_x = \frac{\partial \sigma_x^{(1)}}{\partial x} = \frac{\sigma_z^{(1)}}{R + x} \approx \frac{\sigma_z^{(1)}}{R} \tag{4}$$

The force equilibrium values are defined as solutions of a system of algebraic partial differential equations [11-19]:

$$\begin{cases} \dfrac{\partial \sigma_x}{\partial x}+\dfrac{\partial \sigma_{xy}}{\partial y}+\dfrac{\partial \sigma_{xz}}{\partial z}-F_x=0 \\ \dfrac{\partial \sigma_x}{\partial x}+\dfrac{\partial \sigma_{xy}}{\partial y}-\dfrac{\sigma_z^{(1)}}{R}=0 \\ \dfrac{\partial \sigma_{yx}}{\partial x}+\dfrac{\partial \sigma_y}{\partial y}+\dfrac{\partial \sigma_{yz}}{\partial z}=0 \\ \dfrac{\partial \sigma_{yx}}{\partial x}+\dfrac{\partial \sigma_y}{\partial y}=0 \\ \dfrac{\partial \sigma_{zx}}{\partial x}+\dfrac{\partial \sigma_{zy}}{\partial y}+\dfrac{\partial \sigma_z}{\partial z}=0 \\ \dfrac{\partial \sigma_{zx}}{\partial x}+\dfrac{\partial \sigma_{zy}}{\partial y}=0 \end{cases} \tag{5}$$

Applying the continuity relation of deformation and Hooke's law in an isotropic body, a basic equation for stresses $\sigma_x(x,y)$ and $\sigma_y(x,y)$ is obtained as

$$\nabla^2\left(\sigma_x+\sigma_y\right)=\frac{1}{(1-\nu)R}\cdot\frac{\partial \sigma_z^{(1)}}{\partial x}=\frac{Y}{(1-\nu)R^2} \tag{6}$$

where the differential operator ∇ is in x–y-plane. For solving Equation (6), a stress potential U and a body force potential V are introduced:

$$\begin{cases} \sigma_x=\dfrac{\partial^2 U}{\partial y^2}+V \\ \sigma_y=\dfrac{\partial^2 U}{\partial x^2}+V \\ \sigma_{xy}=\dfrac{\partial^2 U}{\partial x \partial y} \end{cases} \tag{7}$$

$$\begin{cases} F_x=\dfrac{\partial V}{\partial x} \\ F_x=\dfrac{\sigma_z^{(1)}}{R}=\dfrac{Y\left(x+x_0\right)}{R^2} \\ F_y=\dfrac{\partial V}{\partial y}=0 \end{cases} \tag{8}$$

The body force potential is defined to be

$$V = -\frac{Y}{2R^2}\left(x^2 - \frac{d^2}{4}\right) - \frac{Y}{R^2}\left(x - \frac{d}{2}\right) \tag{9}$$

Substituting the variables into (6), a bi-harmonic equation for the stress potential is deduced:

$$\nabla^4 U = -\frac{1-2\nu}{1-\nu}\frac{Y}{R^2} \tag{10}$$

For being valid the solution of Eq. (6) needs to satisfy several conditions. One of them is that the stress and strain are symmetric to the x-axis. At the outer surface of the optical fiber, where the following relation

$$x^2 + y^2 = \frac{d^2}{4} \tag{11}$$

is fulfilled, the stresses σ_y and σ_x are zero at point $x = d/2$. For moderate bending, the deformation of the neutral surface is neglected. This implies that no shear strain exists in the neutral surface (a flat plane at $x = -x_0$). At $x = -d/2$ a certain stress σ_x exists to balance with the reaction force from the ambient mechanical support. As a consequence, the stress potential is defined as

$$U = a\left(x^2 + y^2\right)^2 + b\left(x^2 + y^2\right) + c\left(x^4 - y^4\right) + d\left(x^2 - y^2\right) + exy^2 + fx^3 \tag{12}$$

By applying boundary and symmetry conditions, the stresses are defined as:

$$\begin{cases} \sigma_x = \dfrac{Y}{2R^2}\left[\dfrac{7-6\nu}{8(1-\nu)}\left(x^2 + y^2 - \dfrac{d^2}{4}\right) - \dfrac{1-2\nu}{2(1-\nu)}y^2 + \dfrac{7-6\nu}{4(1-\nu)}x_0\left(x - \dfrac{d}{2}\right)\right] \\ \sigma_y = \dfrac{1-2\nu}{16(1-\nu)}\dfrac{Y}{R^2}\left(x^2 + y^2 - \dfrac{d^2}{4}\right) \\ \sigma_{xy} = \dfrac{1-2\nu}{8(1-\nu)}\dfrac{Y}{R^2}(x + x_0)\,y \end{cases} \tag{13}$$

At the center of the optical fiber, the stresses on the x- and y- axes are defines as:

$$\begin{cases} \sigma_{x0} = -\dfrac{Y}{R^2}\dfrac{7-6\nu}{16(1-\nu)}\left(\dfrac{d^2}{4} + x_0 d\right) \\ \sigma_{y0} = \dfrac{Y}{R^2}\dfrac{1-2\nu}{16(1-\nu)}\dfrac{d^2}{4} \end{cases} \tag{14}$$

Finally, the birefringence is defined as

$$B = -\frac{n^3}{16}\left(p_{11} - p_{12}\right)\left(1+\nu\right)\left[\frac{d^2}{R^2} - \frac{7-6\nu}{2\left(1-\nu\right)}\frac{x_0 d}{R^2}\right] = \\ = -\frac{n^3}{16}\left(p_{11} - p_{12}\right)\left(1+\nu\right)\left[\frac{d^2}{R^2} - \frac{7-6\nu}{2\left(1-\nu\right)}\frac{\overline{e}_z d}{R^2}\right] \tag{15}$$

For the investigated phenomenon, it is important to emphasize that the lateral pressure (mechanical load) applied on the external surface causes a geometric deformation of the fiber core, from a circular area to a slightly elliptical one. According to electromagnetic theory, it leads to a birefringence, a difference of effective refractive indexes between the two axes of the order of 10^{-5}-10^{-6}.

The key parameter to be observed when investigating the SFBG and FBG sensing devices is λ_B, the Bragg resonance wavelength, defined as

$$\lambda_B = 2n_{eff} \cdot \Lambda \tag{16}$$

where Λ is the grating pitch length, n_{eff} is the effective value of the optical fiber core refractive index, which is obtained after some algebra and satisfy the condition

$$n_{clad} < n_{eff} < n_{core} \tag{17}$$

where n_{clad} is the refractive index of the cladding and n_{core} is the refractive index of the core [11-17]. The Bragg wavelength is the peak of the FBG characteristic reflection band. The FBG mode of operation consists mainly of observing the spectral shift of the Bragg wavelength and of the spectral broadening of the Bragg reflection band and of its possible reduction [11-17].

The LPGFS operation is based on fulfilling the Bragg resonance condition [11-19]. The input light beam generated by a broad-spectrum source, thus having an input spectral distribution, is coupled to the SM optical fiber core and propagates guided through the core as the fundamental mode being incident at blaze angle on the LPG and being diffracted by it. An LPG acts as an optical fiber-based grating that favors coupling between the core and the cladding co-propagation modes which is equivalent to an electromagnetic energy transfer from the core mode to the possible propagation cladding modes for which the Bragg resonance condition is fulfilled [15-19]. The transferred energy is lost from the fundamental light mode and appears as absorption bands in the transmission spectrum observed at the SM optical fiber end. The transferred light continues its propagation through the cladding until it is lost into the ambient, kept into a core proximity volume or coupled back, when meeting another LPG, to the fundamental mode. The energy transfer is maximum at discrete wavelengths λ^i defined by the relation [11-19]

$$\lambda^i = \left(n_{eff} - n_{clad}^i\right) \cdot \Lambda \tag{18}$$

where λ^i is the central wavelength of the attenuation band, neff is the effective value of the core refractive index, represents the effective value of refractive index of the i^{th} possible cladding propagation mode and Λ is the period of the LPG. Equation (18) is useful for sensing by observing that the effective values of refractive index of core and cladding propagation modes depend on the ambient refractive index [11-19]. Practically any infinitesimal modification of the light propagation through the LPGFS characteristics is sensed by the LPG and can be observed by the spectral shifting and broadening of each absorption bands induced in SM optical fiber transmission spectrum [11-17]. In the FBG sensor case the mode coupling is induced by the grating between the fundamental mode and counter-propagating ones, a fact imposed by energy and impulse conservation laws, the single noticeable modification of the light spectrum will consist of shifting and broadening of one sharp reflection band centered at λ_B, the Bragg wavelength [11-17].

Regarding Eq. (18), an accurate definition of the effective refractive indexes characteristic for the light propagation modes is necessary. For the core, it is used the Two Layers Model (2LM) of the SM optical fiber based on the assumption that the fiber consists of two concentric cylinders with a step refractive index profile - a uniform core region surrounded by an infinite, homogeneous cladding region of lower refractive index [11-17]. The assumption of an infinite cladding is justified by the exponential nature of decay exhibited by the guided mode outside the core region, which is such that it does not penetrate as far as the cladding-surround boundary in optical fibers - thus making it possible to use an infinite cladding model without undue error [11-17]. Also, 2LM assumes a low core-cladding refractive index difference, so that the fundamental mode can be described in terms of its LP approximation. The dispersion relation for LP_{0m} modes is used and can be written in the following form [11-17]:

$$u_{co}\left(\frac{J_1(u_{co})}{J_0(u_{co})}\right) = w_{co}\left(\frac{K_1(w_{co})}{K_0(w_{co})}\right) \tag{19}$$

where J_0 and J_1 are Bessel functions of the first kind, of zero and first order respectively, and K represents the modified Bessel function of the second kind. u_{co} and w_{co} are the normalized transverse wave numbers that can also be written in terms of the fiber's V -number,

$$V = \frac{2\pi \cdot a_{co}}{\lambda} \cdot \sqrt{n_{co}^2 - n_{cl}^2} \tag{20}$$

where a_{co} is the fiber core radius, λ is the wavelength, n_{co} is the refractive index of the fiber core and n_{cl} is the refractive index of the fiber cladding. The normalized effective index is calculated as it follows [11-17]:

$$b = 1 - \frac{u_{co}^2}{V^2} \approx \frac{n_{effco}^2 - n_{cl}^2}{n_{co}^2 - n_{cl}^2} \tag{21}$$

$$u_{co} = V \cdot \sqrt{1-b} \tag{22}$$

$$w_{co} = V \cdot \sqrt{b} \tag{23}$$

n_{effco} being the effective refractive index of the fiber core. These equations show that u_{co} and w_{co} are only functions of the host fiber's physical parameters, which can be used in conjunction with Eq. (18) to define the core effective refractive index, n_{effco}, such that the condition expressed by Eq. (17) is fulfilled.

Eigenvalues that satisfy the above dispersion relation need to be established numerically. For the correct fiber parameters (such as the core radius, a_{co}, which has a very small value for single mode fiber) only one point of the intersection should occur for the fundamental mode, whose co-ordinates specify the single-valued eigenvalues and thus also the normalized transverse wave numbers. Now since the propagation constant of the fundamental mode can be written in terms of u_{co} and the free-space propagation constant, k, as shown below [8]:

$$\beta_{co} = \sqrt{(k \cdot n_{co})^2 - \left(\frac{u_{co}}{a_{co}}\right)^2} = \sqrt{\left(\frac{2\pi}{\lambda} \cdot n_{co}\right)^2 - \left(\frac{u_{co}}{a_{co}}\right)^2} \tag{24}$$

This means that the effective refractive index of the core can also be determined, since:

$$n_{effco} = \frac{\beta_{co}}{k} = \frac{\beta_{co} \cdot \lambda}{2\pi} \tag{25}$$

For the cladding modes, it is used the Three Layers Model (3LM) of the SM fiber which is based on the assumption that it consists of three concentric cylinders with a step index of refraction profile - a uniform core region surrounded by a much larger (at least by an order of magnitude), homogeneous cladding region of lower refractive index and an by an infinite uniform ambient [11-17]. It is considered that each cladding mode propagation constant is found from a mode dispersion relation in the form of an eigenvalue equation. 3LM can offer a more accurate description of mode propagation in the cladding, for which the cladding modes are not approximated as being linearly polarized. This means that the core-cladding interface cannot be ignored, and the required dispersion relation should incorporate the exact modes corresponding to the three-layer fiber structure, given in [11-17] as:

$$A_0 = A_0' \tag{26}$$

A_0 and A_0' are defined as follows:

$$A_0 = \frac{1}{\sigma_2} \cdot \frac{\left(JK + \frac{\sigma_1 \sigma_2 u_{21} u_{32}}{a_{co} a_{cl} n_{cl}^2} \right) u_2 p_\nu - K q_\nu + J r_\nu - \frac{s_\nu}{u_2}}{-\left(\frac{u_{32}}{a_{cl} \cdot n_{cl}^2} J - \frac{u_{21}}{a_{co} \cdot n_{co}^2} K \right) u_2 p_\nu + \frac{u_{32} q_\nu}{a_{cl} n_{co}^2} + \frac{u_{21} r_\nu}{a_{co} n_{co}^2}} \tag{27}$$

$$A_0{}' = \frac{\sigma_1 \left[\left(\frac{u_{32}}{a_{cl}} J - \frac{u_{21} n_{ext}^2}{a_{co} n_{cl}^2} K \right) u_2 p_\nu - \frac{u_{32} q_\nu}{a_{cl}} - \frac{u_{21} r_\nu}{a_{co}} \right]}{\left(\frac{n_{ext}^2}{n_{cl}^2} JK + \frac{\sigma_1 \sigma_2 u_{21} u_{32}}{a_{co} a_{cl} n_{co}^2} \right) u_2 p_\nu - \frac{K q_\nu n_{ext}^2}{n_{co}^2} + J r_\nu - \frac{s_\nu n_{cl}^2}{u_2 n_{co}^2}} \tag{28}$$

The parameters introduced in Eq. (27) - (28) are defined as:

$$\sigma_1 = j \frac{\nu n_{effcl}}{Z_0} \tag{29}$$

$$\sigma_2 = j \nu n_{effcl} Z_0 \tag{30}$$

$$u_1 = \sqrt{\left(\frac{2\pi}{\lambda} \right)^2 \left(n_{co}^2 - n_{effcl}^2 \right)} \tag{31}$$

$$u_2 = \sqrt{\left(\frac{2\pi}{\lambda} \right)^2 \left(n_{cl}^2 - n_{effcl}^2 \right)} \tag{32}$$

$$w_3 = \sqrt{\left(\frac{2\pi}{\lambda} \right)^2 \left(n_{neffcl}^2 - n_{ext}^2 \right)} \tag{33}$$

$$u_{21} = \frac{1}{u_2^2} - \frac{1}{u_1^2} \tag{34}$$

$$u_{32} = \frac{1}{w_3^2} - \frac{1}{u_2^2} \tag{35}$$

$$J = \frac{1}{2} \cdot \frac{J_{\nu-1}(u_1 a_{co}) + J_{\nu+1}(u_1 a_{co})}{u_1 J_\nu (u_1 a_{co})} \tag{36}$$

$$K = \frac{1}{2} \cdot \frac{K_{\nu-1}(w_3 a_{cl}) - K_{\nu+1}(w_3 a_{cl})}{w_3 K_\nu (w_3 a_{cl})} \tag{37}$$

$$p_\nu = J_\nu (u_2 a_{cl}) N_\nu (u_2 a_{co}) - J_\nu (u_2 a_{co}) N_\nu (u_2 a_{cl}) \tag{38}$$

$$q_\nu = \frac{J_\nu(u_2 a_{cl})\left[N_{\nu-1}(u_2 a_{co}) - N_{\nu+1}(u_2 a_{co})\right]}{2} - \frac{N_\nu(u_2 a_{cl})\left[J_{\nu-1}(u_2 a_{co}) - J_{\nu+1}(u_2 a_{co})\right]}{2} \tag{39}$$

$$r_\nu = \frac{N_\nu(u_2 a_{co})\left[J_{\nu-1}(u_2 a_{cl}) - J_{\nu+1}(u_2 a_{cl})\right]}{2} - \frac{J_\nu(u_2 a_{co})\left[N_{\nu-1}(u_2 a_{cl}) - N_{\nu+1}(u_2 a_{cl})\right]}{2} \tag{40}$$

(41)

In Eq. (27)-(41) $Z_0 = \sqrt{\frac{\mu_0}{\varepsilon_0}} \approx 377\ \Omega$ is the free space electromagnetic impedance, N is defined as a Bessel function of the second kind, and the azimuthal order of the cladding mode is set to $\nu = 1$ for non-zero coupling to occur with the circularly symmetric core mode [11-17].

3. Simulation Results

Both investigated FBG sensor or LPGFS were considered as manufactured into a SM optical fiber considered as standard for communications and sensors, namely Fibercore SM750 type optical fiber, which is, according to literature, commonly used as host for FBG and LPG [11-17]. This means that the optical fiber core has a diameter of 2.8 - 3.5 μm and a refractive index of 1.4585, its cladding has a 62.5 μm diameter with a refractive index of 1.4540 [11-17]. The FBG was considered as having the number of pitches N in the range 1000 - 20000 and a length in the range 1 - 15 mm. The LPGFS was considered as having a length in the range 5 - 70 mm and a grating period in the range 5 - 500 μm. The simulations were performed considering the optical fiber as embedded in Polycarbonate (PC - $(C_{16}H_{14}O_3)_n$) matrix of a composite material.

The first step in performing the FBG or LPGFS simulations consists in defining the effective value of SM optical fiber refractive index in Eqs. (1) and (3).

In Figs. 3 and 4 there are presented the results obtained in calculation of effective value of core refractive index (n_{effco}) and normalized frequency (V_{co}) variations vs the wavelength λ. The effective value of core refractive index is necessary for calculation of Bragg wavelength, the peak wavelength of the FBG characteristic reflection band which is essential for FBG sensing operation. The n_{effco} value allows simulation of Bragg reflection band shape.

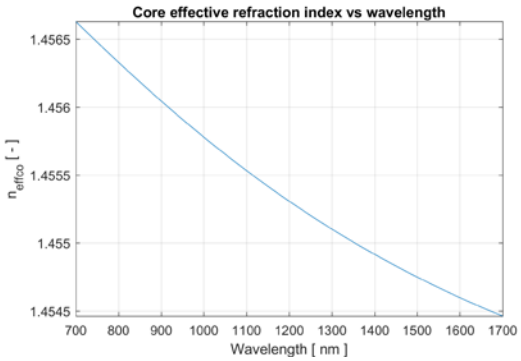

Fig. 3. Simulated variation of core refractive index effective value vs incident light wavelength.

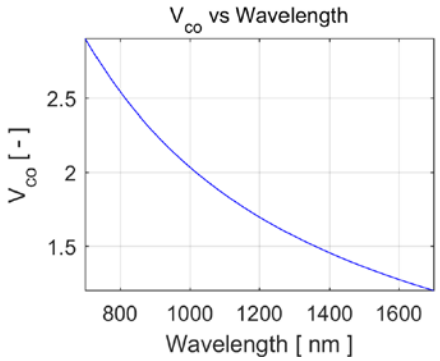

Fig. 4. The variation of core normalized frequency, Vco, as a function of incident light wavelength.

In Fig. 5 there are presented the simulation results accomplished regarding the spectral shift of the Bragg grating reflection spectra obtained for an FBG with length 20 mm and 20000 pitches for detecting a damage produced at a 5 mm distance from the optical fiber axis. In the performed simulation bending is considered the main perturbing effect induced on optical fiber. Bending of the optical fiber is the FBG sensing effect on which its operation is based. Bending of the Bragg grating represents an infinitesimal n_{effco} variation which implies a shift of Bragg reflection band. The initial Bragg reflection band is represented with red and the shifted same band after the defect is induced into polymer matrix is represented with blue. In the investigated case, the Bragg reflection band shift was calculated as 1.895 nm.

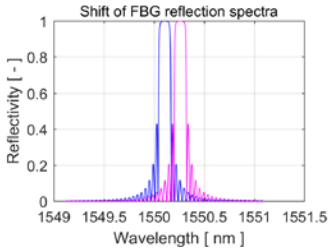

Fig. 5. The simulated shift of FBG (N=20000 pitches and 20 mm length) reflection spectra induced by a crack formed at 5 cm distance from the optical fiber.

For the LPGFS there are two more steps of the simulation procedure directly related to the optical fiber, namely calculation of the variations of cladding refractive index effective values n_{clad}^{i} with wavelength of light propagating through the SM optical fiber core incident on the LPG and of phase matching parametric curves for the first nine cladding propagation modes depending on long period grating period Λ_{LPG} and light wavelength. n_{clad}^{i} was calculated for the first nine cladding modes of light propagation. The calculated n_{clad}^{i} are used for defining the phase matching curves for the investigated LPGFS using Eq. (3). The key of LPGFS operation modes becomes clear after analyzing the significance of the phase matching curves. It can be observed that phase matching curves are parametric curves defined into domains of LPG grating period, Λ_{LPG}, and guided light wavelength. The following procedure was used during the simulations: it is considered a horizontal or vertical line corresponding to a given value of Λ_{LPG} or light wavelength; its intersection points of this horizontal or vertical line with the phase matching curves defines the peaks λ^{i} of absorption bands appearing the optical fiber transmission spectrum. In common cases, for a given Λ_{LPG}, at a wavelength of the emission spectrum of a light source coupled to the LPGFS, corresponds several absorption bands each of them being induced by energy transfer to a cladding propagation mode. The amplitude of these absorption bands decreases with the order of the cladding mode corresponding to its propagation into a larger volume embracing the optical fiber core.

In Fig. 6 there are presented the variations of effective values of refractive index corresponding to the first nine cladding propagation modes simulated for the investigating LPGFS.

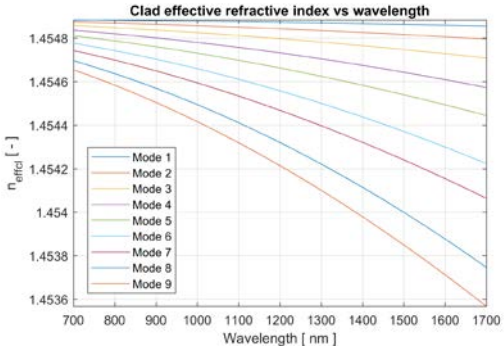

Fig. 6. The variations of cladding refractive index effective values vs incident light wavelength simulated in the LPGFS case.

In Fig. 7 there are presented the variations of phase matching curves. There are presented results simulated for the investigated LPGFS for the first ten cladding propagation modes simulated for the investigating LPGFS. The following procedure is quite simple: imagine a horizontal or vertical line, i.e. corresponding to a given value of Λ_{LPG} or light wavelength; the intersection points of this horizontal or vertical line with the phase matching curves defines the peaks λ^i of absorption bands appearing the optical fiber transmission spectrum. In common cases, for a given Λ_{LPG}, at a wavelength of the emission spectrum of a light source coupled to the LPGFS, corresponds several absorption bands each of them being induced by energy transfer to a cladding propagation mode.

In Figs. 8, 9 and 10 there are presented the results obtained in simulation of damage produced in polymer composite materials using the bending effect induced in LPGFS. During the simulations it was considered the case of a Λ_{LPG} of 650 μm. The absorption peak corresponding to the first cladding propagation mode was calculated to be situated at 980.55 nm and having a bandwidth of 21.76 nm. The bending of the LPGFS induced by the polymer matrix damage is considered the main perturbing effect used for sensing operation.

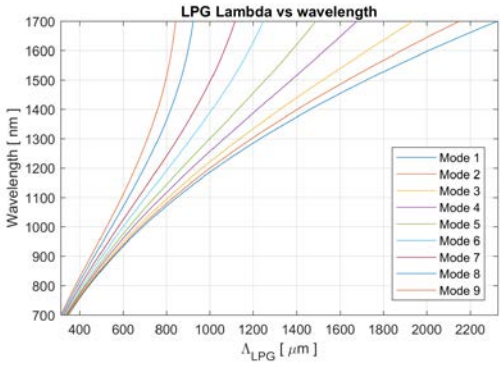

Fig. 7. The phase matching curves with wavelength and with long period grating period length, Λ_{LPG} [μm], simulated for the first nine cladding modes.

In Fig. 8 there is presented the simulation accomplished at absorption band peak located at 980.55 nm and having a bandwidth of 21.76 nm which is shifted at 998.78 nm and broadened to 40.25 nm under the effect of a damage induced in the composite material at distance of 5 mm from the optical fiber axis.

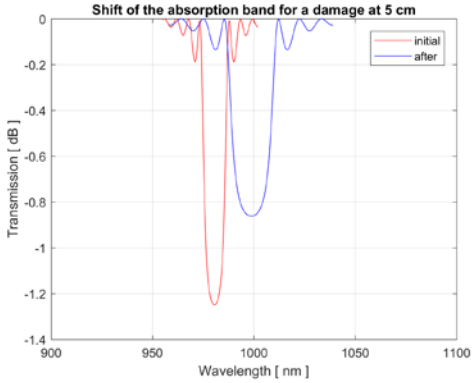

Fig. 8. The spectral shift of the 980.55 nm absorption band peak to 998.78 nm wavelength under the effect of a damage induced in the composite material at a distance of 5 mm.

In Fig. 9 there is presented the simulation accomplished at absorption band peak located at 980.55 nm and having a bandwidth of 21.76 nm which is shifted at 1010.78 nm and broadened to 45.25 nm under the effect of a damage induced in the composite material at distance of 2.5 mm from the optical fiber axis.

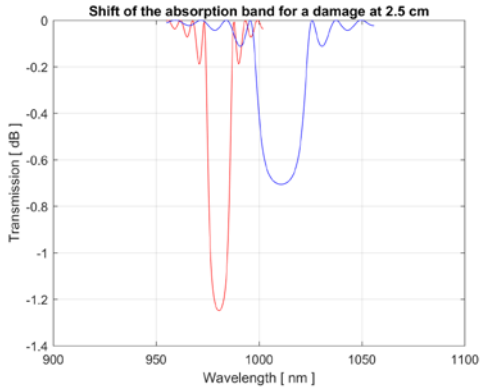

Fig. 9. The spectral shift of the 980.55 nm absorption band peak to 1010.78 nm wavelength under the effect of a damage induced in the composite material at a distance of 2.5 mm.

In Fig. 10 there is presented the simulation accomplished at absorption band peak located at 980.55 nm and having a bandwidth of 21.76 nm which is shifted at 1017.78 nm and broadened to 55.25 nm under the effect of a damage induced in the composite material at distance of 0.5 cm from the optical fiber axis.

As expected, the simulations of the initial absorption band located at 980.55 nm and having a bandwidth of 21.76 nm spectral shifts and broadenings induced by damages of polymer matrix situated at different distances from the optical fiber cannot by synthetized by an analytical relation. The variations of n_{effco} and n_{clad}^{i} on bending radius of curvature and, consequently, of λ^{i}, can be simulated only numerically using very few analytical relations like Eq. (3).

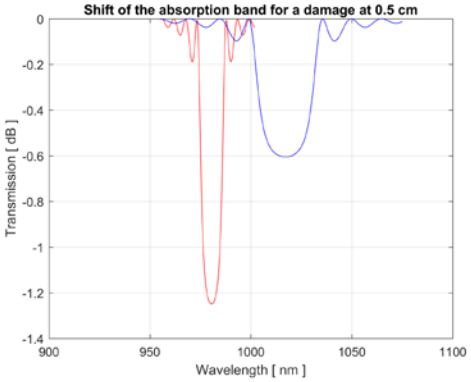

Fig. 10. The spectral shift of the 980.55 nm absorption band peak to 1017.78 nm wavelength under the effect of a damage induced in the composite material at distance of 0.5 mm.

The above presented simulation results refer to static detection of defects induced into the polymer matrix of composite material in which the FBG sensor or LPGFS is embedded. Detection of defects induced into polymer matrix is an important component of any SHM system. It is obvious that a SHM system must observe simultaneously several parameters connected to automotive motion or aircraft flight, among which vibrations types (longitudinal or transversal), frequency and amplitude are very important one. Even only at a qualitatively analysis level, vibrations which are inherent in the operation of a mechanical structure into which parts made of composite materials are mounted represent an important mechanism of defect formation into polymer matrix, mainly cracks and/or voids. This is equivalent to change from the common static analyses made on SM optical fiber sensitivities to a dynamical one. This equivalence is favored by the fact that the FBG sensor and LPGFS response time is five to ten orders of magnitude shorter than the mechanic vibration characteristic times. The FBG sensor and LPGFS response time is practically instantaneous in comparison with the characteristic times of mechanical vibrations. Dynamic influences on physical parameter such as mechanical vibrations should be considered in composite structure design practice. When a vibration in an axial direction occurs somewhere in the SM optical fiber ambient, the deformation will propagate along the fiber to form a longitudinal mechanical wave in its axial direction. Because the fiber is very thin compared to its length and its transverse deformation can occur freely in case of no external force applied on the circumference, the propagation equation is written as is deduced from any classical mechanics textbook. Mechanical vibrations of the structure incorporating parts made of composite materials are investigated as bending mechanisms of optical fibers containing FBG sensors or LPGFS. In this sense, the simulation results presented in Figs. 5, 8, 9 and 10 are examples of experimental situations.

The presented simulation results are accomplished neglecting any possible chemical (thermo-chemical) reaction affecting the polymer matrix structure/composition. The simulation results are in good agreement with the experimental ones reported in literature, for example [20]-[21].

4. Conclusions

For the development of a software package dedicated to automobile SHM, for the composite materials damage detection the bending of optical fiber with FBG or LPGFS is considered as the main mechanism. The investigated FBG sensors or LPGFS were manufactured in a given commercial optical fiber (Fibercore SM 750) and embedded into different types of polymers commonly used as matrix for composite materials. The results obtained in calculations of core and clad effective refractive indexes variations over an extended propagation wavelength range were obtained and used as a starting point of the composite properties simulation process. On this basis, for a given LPG period, there were calculated resonance wavelengths characteristics for several cladding propagation modes. The results obtained in calculation of coupling coefficients of core and cladding propagation radiation modes, followed by the ones obtained in evaluation of absorption coefficients are presented as the simulation next stages. As the final two stages, the transmission spectra, the shift and the bandwidth broadening specific for a resonant wavelength, both induced by a bending deformation of optical fiber, are presented as calculated by using the developed software design package. The simulation results are in good agreement with experimental ones obtained from literature. In subsidiary, the presented results are part of a software design package dedicated to optimization of FBG or long period grating parameters, overall grating length and period, which are to be manufactured into a given single mode fiber, with the environment parameters to be measured with the resulting fiber optic sensor. In this sense, the software design package proves to be useful for calculation of core and clad refractive indexes variations with propagation wavelength, long period grating resonance wavelengths as depending on its period, the absorption coefficients at these resonance wavelengths and consequently, of its transmission spectra. The above mentioned long period grating software design package is under current development, the immediate improvement will consist in using the three layers optical fiber model and in increasing the number of cladding propagation modes used in calculations.

This research is supported by MANUNET grant MNET17/ NMCS0042 and by the Core Program project no. PN 18 28.01.01.

R E F E R E N C E S

[1].*M. Dvorak, M. Ruzicka, V. Kulisek, J. Behal, V. Kafka*, "Damage Detection of the Adhesive Layer of Skin Doubler Specimens Using SHM System Based on Fiber Bragg Gratings", in Procs Fifth European Workshop of Structural Health Monitoring, 2010, pp. 70-75.

[2]. *J. A. Güemes, M. Frövel, J. M. Menendez, F. Rodriguez-Lence, J. Menendez-Martin*, "Embedded fiber Bragg grating as local damage sensors for composite materials", in Procs SPIE **vol. 4694**, Jun. 2002, pp. 1-11.

[3]. *J. R. Lee, C. Y. Ryu, B. Y. Koo, S. G. Kang, C. S. Hong, C. G. Kim*, "In-flight health monitoring of a subscale wing using a fiber Bragg grating sensor system", in Smart Mater Struct, **vol. 12**, no. 1, Jan. 2003, 147-155.

[4]. *A. R. Chambers, N. O. Heinje*, "Damage characterisation in CFRP using acoustic emission, X-Ray tomography and FBG sensors", in Procs. of 17th International Conference on Composite Materials (ICCM-17), 27 - 31 July 2009, Edinburgh, U. K.

[5]. *H. Huang, S. Yuan*, "Composite failure detection in π-joint structure using fiber Bragg grating sensors", in Procs of 2nd Int. Symposium on NDT in Aerospace, Hamburg, Germany, 22-24 Nov 2010.

[6]. *F. P. Camerlingo, G. Cavaccini, A. Ciliberto, C. Voto, M. Iodice, F. Pezzuti*, Alenia SHM Fiber Optic Bragg Grating (FOBG) Strain sensors technology: Applications and Requirements, Alenia Aeronautica, 2006.

[7]. *D. C. Betz, L. Staudigel, M. N. Trutzel, M. Kehlenbach*, "Structural Monitoring Using Fiber-Optic Bragg Grating Sensors", in Struct Health Monit, vol. 2, no. 2, Jun. 2003, pp. 145-162.

[8]. *H. Sekine, S. Fujimoto, T. Okabe, N. Takeda, T. Yokobori*, "Structural health monitoring of cracked aircraft panels repaired with bonded patches using fiber Bragg grating sensors", in Appl Compos Mater, **vol. 13**, no. 2, Mar. 2006, pp. 87-98.

[9]. *D. R. Tenney, J. R. Davis, B. R. Pipes, N. Johnston*, NASA Composite Materials Development: Lessons Learned and Future Challenges, NATO Research and Technology Agency (RTA), Virginia, 2011.

[10]. *G. I. Zagainov, G. E. Lozino-Lozinskii*, Composite Materials in Aerospace Design, Springer, Dordrecht, 1996.

[11]. *D. Savastru, S. Miclos, R. Savastru, I. Lancranjan*, "Numerical Analysis of a Smart Composite Material Mechanical Component Using an Embedded Long Period Grating Fiber Sensor", in Proc SPIE, **vol. 9517**, 95172A, 2015.

[12]. *S. Miclos, D. Savastru, R. Savastru, I. Lancranjan*, "Numerical analysis of Long Period Grating Fibre Sensor operational characteristics as embedded in polymer", in Compos Struct, vol. **183**, no. SI, 2018, pp. 521-526.

[13]. *D. Savastru, S. Miclos, R. Savastru, I. Lancranjan*, "Study of thermo-mechanical characteristics of polymer composite materials with embedded optical fibre", in Compos Struct, vol. **183**, no. SI, 2018, pp. 682-687.

[14]. *S. Miclos, D. Savastru, I. Lancranjan*, "Numerical Simulation of a Fiber Laser Bending Sensitivity", in Rom Rep Phys, **vol. 62**, no. 3, 2010, pp. 519-527.

[15]. *I. Lancranjan, S. Miclos, D. Savastru*, "Numerical simulation of a DFB-fiber laser sensor (I)", in J Optoelectron Adv M, **vol. 12**, no. 8, Aug. 2010, pp. 1636-1645.

[16]. *I. Lancranjan, S. Miclos, D. Savastru, A. Popescu*, "Numerical simulation of a DFB-fiber laser sensor (II) - theoretical analysis of an acoustic sensor", in J Optoelectron Adv M, **vol. 12**, no. 12, Dec. 2010, pp. 2456-2461.

[17]. *R. Savastru, I. Lancranjan, D. Savastru, S. Miclos*, "Numerical simulation of distributed feed-back fiber laser sensors", in Proc SPIE, **vol. 8882**, 88820Y, 2013.

[18]. *S. Miclos, D. Savastru, R. Savastru, I. Lancranjan*, "Design of a Smart Superstructure FBG Torsion Sensor", in Proc SPIE, vol. **9517**, 95172B, 2015.

[19]. *D. Savastru, S. Miclos, R. Savastru, I. Lancranjan*, "Analysis of optical microfiber thermal processes", in Rom Rep Phys, **vol. 67**, no. 4, 2015, pp. 1586-1596.

[20]. *W. Hou, W. Zhang*, "Advanced Composite Materials Defects/Damages and Health Monitoring", in Proc. 2012 Prognostics & System Health Management Conference (PHM-2012 Beijing), MU3102, 2012.

[21]. *X. Zhao, H. Gao, G. Zhang, B. Ayhan, F. Yan, C. Kwan, J. L. Rose*, "Active health monitoring of an aircraft wing with embedded piezoelectric sensor/actuator network: I. Defect detection, localization and growth monitoring", in Smart Mater. Struct., vol. 16, 2007, pp. 1208–1217.